Characterizing CMIP5 model spread in simulated rainfall in the Pacific Intertropical Convergence and South Pacific Convergence Zones

Benjamin R. Lintner[1]*, Baird Langenbrunner[2], J. David Neelin[2], Bruce T. Anderson[3], Matthew J. Niznik[4], Gen Li[5], and Shang-Ping Xie[6]

In preparation for *Journal of Geophysical Research Atmospheres*
26 April 2016

[1]*Rutgers, The State University of New Jersey, New Brunswick, NJ, USA*
[2]*University of California-Los Angeles, Los Angeles, CA, USA*
[3]*Boston University, Boston, MA, USA*
[4]*Rosenstiel School of Marine and Atmospheric Sciences, University of Miami, Miami, FL, USA*
[5]*State Key Laboratory of Tropical Oceanography, South China Sea Institute of Oceanology, Chinese Academy of Sciences, Guangzhou, Guangdong, CHINA*
[6]*Scripps Institution of Oceanography, La Jolla, CA, USA*

Key Points:

1. *Systematic spread in CMIP5 simulation of Pacific region rainfall is investigated using empirical mode reduction techniques.*
2. *Two significant modes of model spread are identified for the DJF rainfall climatology.*
3. *These modes are interpreted in terms of spread in simulated patterns of SST and circulation.*

---

*Corresponding author: Benjamin R. Lintner, Rutgers, The State University of New Jersey, Department of Environmental Sciences, 14 College Farm Road, New Brunswick, NJ 08901-8551, USA
Email: lintner@envsci.rutgers.edu

Abstract. Current-generation climate models exhibit various errors or biases in both the spatial distribution and intensity of precipitation relative to observations. In this study, empirical orthogonal function (EOF) analysis is applied to the space-model index domain of precipitation over the Pacific from Coupled Model Intercomparison Project Phase 5 (CMIP5) simulations to explore systematic spread of simulated precipitation characteristics across the ensemble. Two significant modes of spread, generically termed principal uncertainty patterns (PUPs), are identified in the December-January-February precipitation climatology: the leading PUP is associated with the meridional width of deep convection, while the second is associated with tradeoffs in precipitation intensity along the South Pacific Convergence Zone (SPCZ), the Intertropical Convergence Zone (ITCZ), and the spurious Southern Hemisphere ITCZ. An important factor distinguishing PUPs from the analogy to time series analysis is that the modes can reflect either true systematic intermodel variance patterns or internal variability. In order to establish that the PUPS reflect the former, three complementary tests are performed using preindustrial control simulations: a bootstrap significance test for reproducibility of the intermodel spatial patterns, a check for robustness over very long climatological averages, and a test on the loadings of these patterns relative to interdecadal sampling. Composite analysis based on these PUPs demonstrates physically plausible relationships to CMIP5 ensemble spread in simulated sea surface temperatures (SSTs), circulation, and moisture. Further analysis of atmosphere-only, prescribed SST simulations demonstrates decreased spread in the spatial distribution of precipitation, while substantial spread in intensity remains.

1. Introduction

The tropical Pacific as simulated by state-of-the-art global climate models, including those in Phase 5 of the Coupled Model Intercomparison Project (CMIP5), is characterized by several well-known biases. Prominent among these are the Eastern Pacific cold-tongue bias, with colder than observed sea surface temperatures (SSTs) frequently confined too close to the equator and penetrating too far to the west [*Zheng et al.* 2012; *Li et al.* 2015], and the double Intertropical Convergence Zone (ITCZ), with two bands of deep convection in the east, one on either side of the equator, rather than the observed equatorially asymmetric state with deep convection confined to the Northern Hemisphere only [*Mechoso et al.* 1995; *Li et al.* 2004; *Lin* 2007]. Among the hypotheses accounting for the genesis of biases or errors in eastern tropical Pacific climate are deficiencies in the representation of coupled ocean-atmosphere features or processes, such as spurious warming in the upwelling zone along the South American coast and too strong surface winds and ocean currents [*Zheng et al.* 2012] or larger scale issues related to hemispheric energy imbalances [*Hwang and Frierson* 2013]. Intermodel differences in parameterizations of deep convection as well as clouds, especially low-level marine stratocumuli, may further contribute to errors in simulation of tropical Pacific climate in current generation models [*Mechoso et al.* 1995; *Zhang* 2001; *Lin* 2007; *Brown et al.* 2013].

Perhaps less well-appreciated are the biases occurring outside of the eastern tropical Pacific, particularly those in and around the South Pacific Convergence Zone (SPCZ), a diagonally-oriented convection zone extending from the tropical western Pacific warm pool southeastward into the Southern Hemisphere (SH) midlatitudes of the Central Pacific [*Vincent* 1994]. Coupled models frequently produce SPCZs that are more zonal than observed and with precipitating deep convection penetrating too far into the southeast Pacific dry descent region [*Brown et al.* 2011;

2012; *Ganachaud et al.* 2014; see also Figure 1]. Niznik et al. [2015] stress the importance of distinguishing between the tropical and subtropical portions of the SPCZ when analyzing model bias, given the distinct processes influencing the tropical and subtropical portions. In light of the biases in the eastern equatorial Pacific, it is of interest to quantify how these may affect, or in turn be affected by, the biases in the SPCZ. Moreover, to the extent that biases reflect linkages among components of the climate system, their diagnosis may contribute to understanding why the SPCZ exists, as this remains elusive [*Takahashi and Battisti* 2007; *Power* 2011].

It is noteworthy that the aforementioned biases are little improved from the CMIP3 to CMIP5 model ensembles [*Li and Xie* 2012; *Brown et al.* 2012; *Hirota and Takayuba* 2013; *Li and Xie* 2014]. The continuing occurrence of substantial biases in simulations of present-day climate limits confidence in projections of anthropogenic climate change impacts, especially at the regional scales considered for mitigation and adaptation [*IPCC* 2013]. For example, *Widlansky et al.* [2013] document substantial change in SPCZ region precipitation under future warming, including an equatorward shift of the mean SPCZ axis with amplified 21st century surface warming in the eastern Pacific. For many islands in the Pacific that depend on precipitation from the SPCZ, such shifts would clearly impact water resources and infrastructure, but the errors existing in current climate simulation need to be resolved to meet the needs of planning and decision-making.

An outstanding challenge in model intercomparison, assessment, and validation involves quantifying what may be a range of simulated behaviors across model ensembles. A common approach involves quantifying biases or errors in terms of the model ensemble mean (MEM) and some bulk measure of the spread across the ensemble, e.g., the intermodel standard deviation or root-mean-square difference with respect to the MEM. However, such metrics may fall short of capturing how the models differ with respect to one another other. Our perspective is that the study of systematic differences across a model ensemble may ultimately help to isolate deficiencies in model physics and suggest targets for improvement, beyond what biases or errors in the MEM may already indicate about model deficiencies and how to resolve them. Certainly, in light of the wide array of physical implementations and parameterizations and associated tunable parameters used in current generation models, determining precisely how to correct a particular error may be challenging. Nevertheless, we suggest that the application of methodologies to identify common behaviors in models is useful: at the very least, objective grouping of models based on shared structural features can guide the selection of models for specific applications, such as the design of a multimodel ensemble. As we show below, the methodology we apply here highlights the tendency for models of the same "family" to behave similarly. To the extent that we can consider such similar behavior as reflecting non-independence across these models, one may choose to include only a single representative of a family in an ensemble.

To quantify the spread in simulation of climatological precipitation in the CMIP5 ensemble, we consider here the application of objective empirical mode decomposition techniques to the entire model suite. In the present study, we apply empirical orthogonal function/principal component (EOF/PC) analysis on the space-model index domain rather than the conventional space-time domain. This approach, which we generically term principal uncertainty pattern (PUP) analysis regardless of the specific decomposition technique used, is conceptually similar to recent studies by, e.g., *Deser et al.* [2012], regarding internal variability in a single model ensemble; *Delcambre et al.* [2013a, 2013b]; regarding the Northern Hemisphere jet in the CMIP3 archive; and *Li and Xie* [2012; 2014, with the latter referred to hereinafter as LX14] regarding tropics-wide SST in CMIP3/CMIP5 and tropical Pacific precipitation biases in CMIP5. More recently, *Anderson et al.* [2015] performed a multivariate PUP analysis to relate CMIP5-simulated trends in SST to trends in land surface precipitation, while *Langenbrunner et al.* [2015] applied PUP analysis to identify and attribute CMIP5 model discrepancies in the simulated meridional position and longitudinal extent of the North Pacific storm track in current climate as well as end of the 21st century projections.

2. Data and Methods

We seek here to characterize CMIP5 model spread in simulations of rainfall in the tropical Pacific, focusing on the austral summer (December-January-February) season, when the SPCZ is most prominent. In order to address the impact of coupled ocean-atmosphere versus atmosphere-only sources of model spread, we analyze both the historic (coupled) simulations of CMIP5 as well as stand-alone atmospheric models forced with prescribed sea surface temperature and sea ice boundary conditions [*Taylor et al.* 2012]. The latter follow a protocol similar to the Atmospheric Model Intercomparison Project (AMIP) and are thus referred to hereafter as AMIP-style simulations. For the historic suite, 36 models are analyzed; for the AMIP-style suite, 30 models are analyzed. The models and associated acronyms are summarized in Table 1. For each available model, we use only a single ensemble member, to give equal weighting to each model in the analysis. For ease of comparison, all model fields are first regridded using bilinear interpolation to a uniform 2.5º x 2.5º grid over a rectangular domain spanning 120ºE–60ºW and 50ºS–20ºN. For both the historic and AMIP-style simulations, 27 years of data for December-January-February (DJF) are analyzed, spanning the common period 1979-2005. Of course, the AMIP simulations are forced with observed SSTs while the historic simulations have SSTs that freely evolve subject to prescribed forcings from insolation, volcanic eruptions, and anthropogenic emissions. As we elaborate on further below, the behavior we identify is robust to the sampling time period.

Precipitation climatologies for both the coupled and AMIP-style ensembles are concatenated to form $M \times N$ matrices, where M denotes the spatial dimension (i.e., $M = Mx \times My$ longitude-latitude points) and N the model index dimension; EOFs and PCs are computed from this $M \times N$ matrix. The resulting modes (or PUPs) capture the leading spatial patterns of intermodel differences in terms of variance explained across the space-model index domain. The PC associated with each PUP corresponds to the loadings (or projections) of individual model climatologies onto that spatial pattern (EOF), providing an indication of the relative contribution of each model to that PUP. For example, a large positive loading or PC value for a given model means that it projects strongly (and positively) onto that mode, relative to the ensemble mean. These weights are further used as the basis for regression analysis of various fields related to precipitation, including SST, winds, and moisture.

We have also applied maximum covariance analysis (MCA) to the cross-covariance matrix of precipitation and SST. The MCA-based approach yields pairs of uncertainty patterns for precipitation and SST representing coupled ensemble spread in these two fields. For more information on these methods, the reader is referred to *Langenbrunner et al.* [2015] and the references therein.

3. Results

3.1 PUPs for coupled model simulations

In computing the PUPs, we seek to identify systematic variation in model behavior relative to the MEM. Thus, for reference, Figure 1 shows DJF MEM precipitation for the historic simulations as well as the departure of the MEM from the observations, in this case from the Global Precipitation Climatology Project [GPCP; *Adler et al.* 2003]. Several aspects of the rainfall biases discussed in Section 1 are readily apparent. For example, the MEM is too wet in the SH Eastern Pacific, reflecting the model simulation of a spurious SH ITCZ there, while the dipole appearing along the poleward portion of the SPCZ is consistent with its too zonal orientation in the models. Along the equator, especially to the west of the International Dateline, the MEM considerably underestimates rainfall relative to GPCP, consistent with too cool SSTs and excessive westward extension of cold tongue [*Li et al.* 2015; 2016]. Farther to the west near the Maritime continent, the CMIP5 models are excessively wet, as they also are over the western coast of South America. An important caveat in discussing these biases is that different observational products may yield divergent estimates of rainfall. For example, the GPCP estimates of precipitation are lower over much of the tropical and subtropical ocean, especially in the west Pacific, compared to the Climate Prediction Center (CPC) Merged Analysis of Precipitation [CMAP; *Xie and Arkin* 1997] data set, which has been attributed to use of atoll-based rain gauge estimates in the latter but not in the former [*Yin et al.* 2004]. While differences across observational estimates are clearly important in validating model performance, for our purposes in understanding the spread of CMIP5 simulations relative to the MEM, they are not critical.

3.1.1 FIRST PUP

For the PUPs computed from the *N* = *36* coupled model DJF precipitation climatologies, the leading two modes emerge as well separated from the remaining modes and are thus regarded as significant according to the method of *North et al.* [1982]. The first mode, which accounts for 24.3% of the total field variance, is depicted in Figure 2a. The leading PUP predominantly captures the CMIP5 historic ensemble's spread in the meridional width of principal centers of Pacific region deep convection. Within the SPCZ, the leading mode exhibits its largest positive loadings slightly equatorward of the mean diagonal axis through the mean precipitation centroid over 5ºS to 15ºS; the ITCZ is similarly split. The gray 4 mm day^{-1} contours, representing averages over models with positive (solid) and negative (dashed) loadings (see Figure 2b), underscore the spatial displacements of the SPCZ and ITCZ between the two subsets of models.

Comparing the leading PUP to the MEM bias relative to GPCP (Figure 1b) indicates little systematic relationship between the spatial patterns. For example, along the poleward margin of the ITCZ and along the equator just west of the Dateline, the positive weight models have reduced bias compared to the models with negative weights. On the other hand, the models with positive weights exhibit an enhanced spurious SH ITCZ, which is especially evident in the 4 mm day^{-1} contour. Such behavior underscores a difficulty in bias correction, namely that alleviation in one region is often associated with degradation in another [*Wang et al.* 2014].

The ACCESS and HADGEM2 families of models exhibit the largest positive model weights, corresponding to a narrower ITCZ/SPCZ complex with precipitation more concentrated along the equator, while the MPI models exhibit the largest negative weights, corresponding to a wider ITCZ/SPCZ. Overall, the model weights for simulations from the same parent are typically close. The effective degrees of freedom [*Bretherton et al.* 1999] estimated from the variance spectrum of the EOF modes is ~9. The tendency for similar values of model weights for sibling models is consistent with a lower number of degrees of freedom in the ensemble, since not all models within the ensemble are independent. However, it is not always the case that siblings are close, e.g., two of versions of the IPSL models exhibit modest negative loadings with respect to PUP 1 while the third is positively loaded. In this case, the two negative weight models share the same convection scheme (differing otherwise in terms of horizontal resolution), while the third has a distinct convection scheme [*Oueslati and Bellon* 2013].

Obviously, it is necessary to assess whether the PUPs represent physically plausible behavior or merely mathematical artifacts of the methodology: after all, it is possible that the spatial structure occurs with no clear relationship to underlying physical processes. To provide some physical context, we linearly regress various climate fields from the models using the leading mode PC (model weights) as the regression index; in Figure 2c, we present the results of the regression analysis for SST and 850 mb winds. The values shown correspond to unit standard deviation scaling of the PC, i.e., a model weight of +1.

From the SST regression, the near-equatorial enhancement of rainfall in PUP mode 1 is associated with a widespread region of SSTs in the Central to Eastern Pacific ~0.5-0.75 °C warmer than the MEM (again, assuming a model weight of +1). The warm SSTs both underlie the enhanced rainfall and extend to the east of the principal near-equatorial positive precipitation values evident in Figure 2a. The spatial patterns of rainfall and SSTs are qualitatively consistent with interannual variability associated with El Niño/La Niña events in both observations and models [*Folland et al.* 2002]. Thermodynamically, the occurrence of warmer than MEM SSTs over a broad region upstream, as defined based on the orientation of the mean low-level trade wind inflow, should increase low-level moist static energy (MSE), both through low-level warming and moistening. Thus, models with higher low-level MSE compared to the MME may be expected to support rainfall further to the east [*Lintner and Neelin* 2008; *Niznik and Lintner* 2013].

Considering the mode 1 regression of 850 mb winds, the meridional pattern of drier conditions toward the poles and wetter conditions toward the equator is associated with anomalous low-level convergence. Moreover, within the equatorward region of enhanced leading mode rainfall, the low-level winds are anomalous northwesterly. Since the climatological DJF low-level circulation in this region is southeasterly to easterly, the low-level winds in models favoring higher rainfall along the equator are therefore weakened. We point out here consistency with the physical mechanism for variability at the margins of tropical deep convection zones discussed by *Lintner and Neelin* [2008] and *Niznik and Lintner* [2013], in which enhanced moisture and precipitation along the eastern margin of the SPCZ was related to reduced dry air (or low-MSE) advection associated with slackened trade winds from the dry and cool, low MSE region upstream. Moreover, the principal axis of low-level winds along the SPCZ coincides with enhanced rainfall extending southeastward toward SH midlatitudes for the models with positive weights; this behavior suggests outflow of moisture along the SPCZ in these models is important for sustaining convection on its poleward edge. In the extreme southeast Pacific, the low-level winds in Figure 2c are associated with an anomalous cyclonic circulation opposing the quasi-stationary climatological mean anticyclone (the South Pacific High) located there. Regressions of specific humidity at 700 mb and winds at 200 mb (not shown) also support these results.

An important distinction between the PUP analysis presented here and conventional EOFs calculated across a time series is that the PUP modes can arise from two sources of variance: internal climate variability in individual models and true intermodel variability. Prior work (e.g., *Deser et al.* [2012]) indicates that internal variability can lead to distinct regional behavior in climatologies over timescales comparable to the 27-year means for our PUP analysis. For example, in the Pacific, models simulate well-known low-frequency modes of observed variability like the Pacific Decadal Oscillation (PDO) or the Interdecadal Pacific Oscillation (IPO), but the phase of these is dependent on the model initialization [*Anderson et al.* 2015]. Since the spatial footprint of the PDO (or IPO) on SST in the tropical and southern Pacific is somewhat reminiscent of the SST regression in Figure 2c, distinguishing between internal (sampling) variability and systematic intermodel variability requires careful attention, and we have addressed this in three separate and complementary ways.

First, we employed a bootstrapping technique to provide a significance test for the pattern in Figure 2a. This was done by generating 100 randomized 30-year climatologies from 5-year segments in the preindustrial control runs (see Table 1 for more information). This procedure yielded 100 'alternative' ensembles, and a PUP analysis was performed on each. The average spatial correlation between the leading modes from this set of 100 alternative ensembles and that in Figure 2a is $r = 0.95$, implying that the pattern seen in Figure 2a is robust to sampling. A two-sided t test was further applied at each grid point to these modes to assess whether the sample means of grid point values among the 100 bootstraps are significantly different from zero. The results of this test are stippled where grid points pass at the 99% confidence level in Figure 2a, indicating widespread confidence that the leading mode does not arise from sampling of interdecadal variability.

As a second check that the results in Figure 2a are not the result of internal variability, we calculated the climatology of the preindustrial control run simulation for each model over its *entire* length (ranging from 240 to 1050 years): that is, we check whether the spatial pattern seen in Figure 2a is reproducible for climatologies much longer than 30-year averages. The spatial correlation between the 1st PUP (not shown) and Figure 2a is r = 0.95, with similar percent variance accounted for, indicating that this PUP is also distinct from sampling across low-frequency (on the order of 100 years or longer) oscillations.

A final test can be seen in the error bars in Figure 2b. Consecutive, non-overlapping 30-year climatologies from the preindustrial control runs were calculated for each model, and the resulting climatologies were centered by the 1979-2005 ensemble mean and projected onto Figure 2a. The error bars in Figure 2b represent the range of values for these projections, or a measure of internal variability of the principal components. The spread for each model is notably smaller than that across the entire ensemble, indicating that internal model variability is not a major contributor to the pattern in Figure 2a.

Taken together, this set of checks leads us to conclude that the PUP in Figure 2a represents true systematic differences across model climatologies, distinct from internal model variability.

3.1.1 SECOND PUP

The 2nd mode PUP for the historic ensemble, accounting for 16.9% of the field variance, is presented in Figure 3. The predominant feature of this PUP is widespread occurrence of positive values outside of the central and eastern Pacific, with especially large values in the SPCZ and to the north of Australia (Figure 3a). By contrast, the 2nd PUP reflects strong negative values over the spurious SH ITCZ as well as in the upwelling region adjacent to the coast of South America. The spatial tradeoff in precipitation intensity between the SPCZ and ITCZ can be interpreted qualitatively in terms of a teleconnected atmospheric response to diabatic (convective) heating, as in the *Gill* [1980] model. That is, those models which exhibit stronger convection over the

SPCZ may be expected to simulate weaker precipitation elsewhere (such as over the eastern Pacific) through mass balance of stronger ascent in the SPCZ and stronger subsidence elsewhere. We point out that the areas enclosed by the 4 mm day^{-1} contour are approximately the same for both the positive and negative weight models, which is consistent with the notion of a spatial redistribution of rainfall within the domain. The regression analysis (Figure 3c) highlights SSTs colder than the MEM collocated with the largest negative rainfall values in the eastern tropical Pacific.

Our leading PUP modes are in general agreement with the results of LX14 (c.f., their Figure 2), which depict regressions of precipitation, SST, and surface winds onto PCs of intermodal spread in annual- and zonal-mean tropical Pacific rainfall, normalized with respect to each model's tropical mean rainfall, for a smaller set (N = 18) of CMIP5 models. LX14 remark that similar results were obtained for the decomposition over longitude and latitude, which would be more directly comparable to our analysis. There are, however, some differences with respect to LX14. For instance, the leading PUP from our analysis accounts for less than half the variance compared to the leading mode of LX14. This difference may stem from the normalization applied in LX14, which may be expected to suppress some of the spread across models, given model-to-model differences in the overall amount of tropical rainfall, thereby increasing the variance captured by the leading mode in LX14. The 2nd mode of LX14 manifests a much more pronounced dipole in the regression of precipitation over the eastern north tropical Pacific than is evident in our 2nd mode. However, analysis of the PUPs computed on the June-July-August (JJA; not shown) climatology indicates a similarly located dipole appearing in the second JJA PUP (with similar overall structure to the second mode for DJF). Thus, there is some modulation of the spatial details by the choice of season. Overall, though, the similarity of the leading PUPs to the results of LX14, obtained with some differences in the underlying methodology and selection of models and analysis period, supports the robustness of these patterns of model spread.

As with the leading mode, we checked the reproducibility of the pattern in Figure 3a against sampling variability: using the bootstrap method, the spatial correlation between 100 bootstrapped 2nd PUP modes and that of Figure 3a is $r = 0.94$. The stippling throughout Figure 3a underscores that the behavior at most gridpoints is distinct from internal variability, and the small error bars on model weights in Figure 3b show that within-model spread is small compared to the spread across the ensemble. Finally, the 2nd PUP calculated from climatologies computed over the entire preindustrial control time series produces a spatial correlation of $r = 0.94$. We therefore reiterate that the second mode is distinct from sampling internal variability at decadal or longer time scales.

It is interesting to note that while the 1st and 2nd PUP PCs are uncorrelated in a linear least squares sense (by construction), they do exhibit an apparent higher-order relationship (Figure 4). In particular, using a quadratic fitting function yields a correlation of 0.54 between the two PCs. Rejecting the obvious outliers (the CSIRO, CMCC-CMS and CMCC-CESM, GISS models) further increases the quadratic best fit (r = 0.78) without significantly changing the linear correlation. The quadratic relationship between the model weights for the first two modes implies that models with strong SPCZ regional rainfall (2nd PC > 0) may have either relatively narrow (PC > 0) or wide (PC < 0) meridional distributions of rainfall, while models with weak SPCZ region rainfall tend to fall closer to the ensemble-mean with respect to the overall latitudinal extent of Pacific region convection.

3.2 MCA and relationship of coupled model precipitation spread to SST

As noted above, within coupled models, biases are often attributed to poor simulation of ocean dynamics. With respect to simulated precipitation, errors arising from ocean dynamics may impact SSTs, which in turn induce errors in surface fluxes and ocean-atmosphere coupling that affect temperature and moisture vertical structure in the overlying atmosphere. To investigate this linkage, we applied Maximum Covariance Analysis (MCA) to the cross-covariance matrix of normalized precipitation and SST for the historic simulations, as shown Figure 5. The leading MCA mode accounts for 66% of the total squared covariance between these two fields, with a correlation coefficient between the model weights for the precipitation and SST fields of r = 0.79, implying tight coupling between the model spread in precipitation and SST. The squared covariance value is significant at the 94% confidence interval, based on a Monte Carlo procedure with a sample size of 300. The precipitation pattern associated with the spatial projection of the first MCA mode manifests a horseshoe-like pattern reminiscent of the leading coupled PUP mode in Figure 2a; in fact, the spatial pattern correlation coefficient between the leading coupled model EOF- and MCA-based PUPs is 0.78, while the model weights for these PUPs are correlated with r = 0.88. One difference in the precipitation field of the MCA-based PUP relative to the 1st EOF-based PUP is that the former exhibits large values in the vicinity of the spurious SH ITCZ (around 120°W, 10°S); in this regard, the leading SVD precipitation pattern more resembles the 2nd EOF-based PUP. Indeed, the spatial correlation pattern coefficient (r = 0.35) and the correlation of model weights (r = 0.32) for the 2nd precipitation EOF PUP and leading MCA PUP are both significant at p = 0.05.

3.3 PUPs for AMIP-style simulations

We have also analyzed the spread across ensemble members for the AMIP-style simulations. Analogous to Figure 1, Figure 6 depicts the DJF MEM precipitation for the AMIP ensemble as well as the bias relative to GPCP. Overall, there is an improved spatial distribution of precipitation over the domain, with the spurious SH ITCZ effectively eliminated and the slope of the SPCZ improved, although the tilt of the more subtropical portion is still somewhat too zonal. Also, the intensity of rainfall within the SPCZ and ITCZ is generally larger than the GPCP values. Interestingly, in comparison to the coupled models, the bias actually worsens along the northern margin of the extreme eastern portion of the ITCZ: a possible explanation for the degradation of the AMIP simulations in this region is that competition for convection between the NH and SH ITCZs in the coupled simulations suppresses intensity to the north, leading to values more in line with GPCP.

For the AMIP-style ensemble, the spread across ensemble members arises from poor parameterizations or missing physics within the atmosphere only, since the same boundary conditions (SSTs and sea ice) are prescribed across the models. A gross comparative measure of the total variability within that selection of models for each of the historic and AMIP-style ensembles can be obtained from the sum of squares of the elements in the covariance matrix (the Frobenius norm; see *Bretherton et al.* 1992), which we normalize by the number of models in each ensemble to account for the different number of models. For the coupled ensemble, the (normalized) Frobenius norm is ~1855 mm^2 day^{-2}, while it is ~1190 mm^2 day^{-2} for the AMIP-style simulations. The larger intermodel variability within the coupled ensemble is consistent with additional sources of uncertainty owing to coupling of the atmosphere to an interactive ocean. Nevertheless, that the total variance in the AMIP models is ~2/3 as large as in the fully coupled versions indicates that atmospheric processes alone contribute substantially to ensemble spread.

Figure 7 depicts the leading EOF-based PUP for the AMIP-style simulations. This mode explains 23.4% of the total variance, i.e., comparable to mode 1 for the historic ensemble. For the AMIP PUPs, only the leading mode is well separated from the remaining modes. Overall, the leading AMIP PUP spatial pattern highlights model discrepancies localized primarily over the western portion of the domain where simulated precipitation values are largest: models with positive loadings exhibit larger than MEM rainfall over the SPCZ and lower values to the north in the ITCZ as well as over northern Australia. The latter region is characterized by a summer monsoon climate. Prior work [e.g., *Kiladis et al.* 1989; *Mantsis et al.* 2013] points to coupling with the Australian summer monsoon as an important determinant of SPCZ intensity and spatial structure, especially in its more tropical portion. This linkage is consistent with the structure in the leading PUP, in that models with enhanced precipitation in the SPCZ tend to simulate reduced precipitation in the Australian monsoon region. As with the leading mode of the coupled ensemble, the regression of model weights for the leading AMIP PUP onto 850 mb winds indicates stronger (north)westerlies in models with more intense rainfall in the SPCZ.

Relative to the historic coupled ensemble, the MEM DJF 4 mm day^{-1} precipitation for the AMIP-style simulations more closely approximates the location of the observed 4 mm day^{-1} contour, demonstrating improved fidelity among the AMIP-style simulations in capturing the overall spatial distribution of precipitating deep convection in the Pacific domain. That is, the specification of the boundary forcing through imposed SSTs leads to a better match to observed rainfall distribution. The spatial pattern correlations of the leading AMIP PUP modes with respect to the 1st and 2nd historic EOFs are 0.63 and 0.22, respectively. Thus, errors or uncertainties in simulations of the atmosphere itself may be viewed as contributing to the spatial pattern of the leading coupled mode, in addition to the structural differences associated with fully coupled ocean-atmosphere dynamics. Some caution is warranted in comparing the results, given the different models assessed in the coupled and AMIP-style simulations. Still, for the subset of models common to both the coupled and AMIP-style ensembles ($N = 25$), the correlation between model weights of the leading PUPs is 0.49, which is significant at $p = 0.05$. This correlation remains significant at the 95th percentile even if reasonable allowance is made for a lower number of degrees of freedom owing to non-independent models.

3.4 PUPs for precipitation standard deviation

In addition to computing PUPs for the DJF precipitation climatologies, we have also computed PUPs with respect to simulation of the interannual standard deviation in the coupled historic simulations (Figure 7). The two leading variability PUPs account for 30.3% and 16.9%, respectively, and are well separated from the remaining modes. The first mode (Figure 8a) identifies spatially pervasive differences in the level of variability across the model ensemble. On the other hand, the second mode (Figure 8b) emphasizes models with high or low variability along the equator in the central Pacific. Given the localization of the 2nd mode to the principal region of ENSO variability, it suggests spread arising from model simulation of ENSO and atmosphere-ocean feedbacks within this region. Indeed, there is modest correlation between the model weights for the 2nd mode and SST variability in the NINO3 region (not shown).

Perhaps not surprisingly, the weights for the historic ensemble climatology and standard deviation PUPs exhibit some relationships. Both the 1st and 2nd PUP model weights for the historic climatology are positively correlated (at $p = 0.05$) with the model weights of the leading

PUP for standard deviation, i.e., the models exhibiting more intense climatological precipitation along the equator and/or along the SPCZ tend to be those with higher interannual standard deviations, i.e., areas with higher mean rainfall experience a greater degree of year-to-year variability. On the other hand, model weights for the 2^{nd} historic climatology PUP are negatively correlated with those of the 2^{nd} standard deviation PUP, i.e., models with higher rainfall interannual variability over the equatorial central Pacific tend to have a more pronounced climatological double ITCZ, but less intense rainfall toward the axis of the SPCZ.

For completeness, we have further computed PUPs on the DJF interannual precipitation standard deviation for the AMIP-style simulations (not shown). The leading mode, which accounts for 38.4% of the variance, strongly resembles the leading mode for the historic ensemble (Figure 7a), again showing pervasive differences across the models in the overall level of precipitation variability and pointing to uncertainties in representation of atmospheric processes as the principal determinant of this aspect of model spread. On the other hand, no analogue to the historic ensemble 2^{nd} mode PUP (Figure 8b) is evident in the AMIP-style ensemble, which underscores the role of ocean-atmosphere coupling in generating this aspect of the interannual variability in the models.

4. Summary and discussion

In this study, we have applied an approach, generically termed principal uncertainty pattern (PUP) analysis, to investigate the leading patterns characterizing the spread among CMIP5 model simulations of DJF tropical Pacific precipitation. The two leading PUPs for the historic (coupled ocean-atmosphere) simulations, derived from EOF/PC analysis, reveal distinct patterns of differences of the models with respect to ensemble mean in both the spatial distribution of precipitation as well as its intensity. The first mode can be broadly characterized in terms of spread in the meridional width of the Pacific ITCZ-SPCZ complex as well as the zonal distribution of precipitation along the equator. The second mode shows spread expressed as a tradeoff between SPCZ and ITCZ precipitation intensity, the latter including the spurious SH ITCZ.

As we have noted, PUPs may reflect either true intermodel spread or internal variability, which is quite distinct from application of EOFs (or other methods) in the time domain. Thus, an important consideration is how to distinguish these two potential sources of PUP behavior. To address this, we performed a bootstrap significance test for the intermodel spatial patterns, a test on the model weights, and a check for robustness against longer climatological averages. The results confirm in complementary ways that these patterns in fact arise from intermodel differences in the tropical Pacific climatology and are distinct from internal model variability at times scales of several decades or longer.

Simple linear regressions of SST and low-level circulation (as well as humidity) onto precipitation PUP model weights underscore the physical consistency of these interpretations, as does application of maximum covariance analysis (MCA) to the covariance matrix of precipitation and SST. By analyzing the stand-alone atmospheric (AMIP-style) simulations in which the impacts of SST-related biases are suppressed, intermodel spread in rainfall intensity remains, especially in the western tropical Pacific, even as the overall spatial configuration of domain-wide precipitation is improved.

While we have demonstrated the plausibility of the precipitation PUPs in terms of their physical consistency with other climate fields, can we draw any conclusions about the source of spread as it relates to particular aspects of model parameterizations, especially for the AMIP-style models for which errors related to ocean dynamics are suppressed? One way of interpreting the spatial structure inherent to the leading AMIP PUP (Figure 7a) is that it corresponds to model tradeoffs in precipitation in the SPCZ core compared to the margins, i.e., models with more intense precipitation have narrower SPCZs.

In prior work using an intermediate level complexity model, *Lintner et al.* [2012] described a pattern of reduced precipitation along the margins and enhanced precipitation in the cores of strong tropical convection zones with the addition of an entrainment-like process to the model's convection scheme. The occurrence of this spatial pattern was tied to dry air mixing reducing convective available potential energy along the margins; the enhanced precipitation in the interior was related to enhanced moisture converging within the convection zone core. *Oueslati and Bellon* [2013] documented similar behavior in entrainment sensitivity experiments in the family of CNRM models, as did *Hirota et al.* [2014] in MIROC5 simulations with different representations of entrainment.

It remains to be seen whether the PUP model weightings can be systematically related to entrainment or other parameterized processes. On this note, *Siongco et al.* [2014] applied an object classification method to sort CMIP5 AMIP-style models into two groups, depending on where these models exhibited the strongest bias in the Atlantic ITCZ; they found no systematic relationship between the location of bias and the convective parameterization used. A practical challenge is that comprehensive documentation of parameter values for CMIP5 models is difficult to obtain. We did examine model weightings for the 1st AMIP PUP with respect to qualitative descriptors of model components available from the Earth System Documentation website (http://compare.es-doc.org/) but this revealed no clear source of spread.

In future work, we anticipate continuing application of PUPs as a tool for diagnosing sources of model ensemble spread in precipitation and how these relate across different variables. For example, *Bellucci et al.* [2010] and *Oueslati and Bellon* [2015] have speculated that overestimation of the occurrence frequency of weak or moderate ascent regimes in the CMIP5 ensemble, rather than precipitation intensity within different vertical velocity regimes, principally accounts for the simulated precipitation errors in these models. Thus, inclusion of the vertical motion field in the MCA may be instructive. We also envision application of PUPs to single model ensembles in which a parameter or set of parameters is systematically varied. By doing so, we can assess the extent to which variations in different parameters may produce distinct spatial patterns of model disagreement.

Acknowledgments

CMIP5 data were obtained from the Program for Climate Model Diagnosis and Intercomparison (PCMDI) data portal [http://cmip-pcmdi.llnl.gov/cmip5/data_portal.html]. BRL and MJN acknowledge the financial support of NSF-AGS-1312865, JDN and BL acknowledge the support of NSF-AGS-1540518 and NOAA NA14OAR4310274, and GL acknowledges the support of the Youth Innovation Promotion Association CAS and the Guangdong Natural Science Funds for Distinguished Young Scholar (2015A030306008).

References Cited

Adler, R. F., G. J. Huffman, A. Chang, R. Ferraro, P. Xie, J. Janowiak, B. Rudolf, U. Schneider, S. Curtis, D. Bolvin, A. Gruber, J. Susskind, and P. Arkin, 2003: The Version 2 Global Precipitation Climatology Project (GPCP) Monthly Precipitation Analysis (1979-Present). *J. Hydrometeor., 4*,1147–1167.

Anderson, B.T., B.R. Lintner, B. Langenbrunner, J.D. Neelin, E. Hawkins, and J. Syktus, 2015: Sensitivity of terrestrial precipitation trends to the structural evolution of sea surface temperature. *Geophys. Res. Lett., 42*, 1190—1196, doi:10.1002/2014GL062593.

Bellucci, A., S. Gualdi, and A. Navarra, 2010: The double-ITCZ syndrome in coupled general circulation models: The role of large-scale vertical circulation regimes. *J. Clim., 23*, 1127–1145.

Bretherton, C. S., C. Smith, and J. M. Wallace, 1992: An Intercomparison of Methods for Finding Coupled Patterns in Climate Data. *J. Clim., 5*, 541–560.

Bretherton, C. S., M. Widmann, V. P. Dymnikov, J. M. Wallace, and I. Bladé, 1999: The Effective Number of Spatial Degrees of Freedom of a Time-Varying Field. *J. Clim., 12*, doi:1175/1520-0442.

Brown, J. R., S. B. Power, F. P. Delage, R. A. Colman, A. F. Moise, and B. F. Murphy, 2011: Evaluation of the South Pacific Convergence Zone in the IPCC AR4 climate model simulations of the twentieth century. *J. Clim.*, *24*, 1565–1582.

Brown, J. R., A. F. Moise, and F. P. Delage, 2012: Changes in the South Pacific Convergence Zone in IPCC AR4 future climate projections. *Clim. Dyn., 39*, 1–19.

Brown, J. R., A. F. Moise, and R. A. Colman, 2013: The South Pacific Convergence Zone in CMIP5 simulations of historical and future climate. *Clim. Dyn., 41*, 2179–2197, doi: 10.1007/s00382-012-1591-x.

Delcambre, S. C., D. J. Lorenz, D. J. Vimont, and J. E. Martin, 2013a: Diagnosing Northern Hemisphere Jet Portrayal in 17 CMIP3 Global Climate Models: Twentieth Century Variability, *J. Climate*, 26, 4910–4929.

Delcambre, S. C., D. J. Lorenz, D. J. Vimont, and J. E. Martin, 2013b: Diagnosing Northern Hemisphere Jet Portrayal in 17 CMIP3 Global Climate Models: Twenty-First-Century Projections, *J. Climate*, 26, 4930–4946.

Deser, C., A. S. Phillips, V. Bourdette, and H. Teng, 2012: Uncertainty in climate change projections: The role of internal variability. *Clim. Dyn., 38*, 527–546, doi:10.1007/s00382-010-0977-x.

Folland, C. K., J. A. Renwick, M. J. Salinger, A. B. Mullan, 2002: Relative influences of the Interdecadal Pacific Oscillation and ENSO on the South Pacific Convergence Zone. *Geophys. Res. Lett.*, *29*, Art #1643.

Ganachaud, A., et al. (2014), The Southwest Pacific Ocean circulation and climate experiment (SPICE), *J. Geophys. Res. Oceans, 119*, 7660–7686, doi:10.1002/2013JC009678.

Gill, A. E., 1980: Some simple solutions for heat induced tropical circulation. *Q. J. R. Meteorol. Soc., 106*, 447–462.

Hirota N., Y. N. Takayabu, M. Watanabe, and M. Kimoto, 2011: Precipitation reproducibility over tropical oceans and its relationship to the double ITCZ problem in CMIP3 and MIROC5 climate models. *J. Clim., 24*, 4859–4873.

Hirota, N., and Y. N. Takayabu, 2013: Reproducibility of precipitation distribution over the tropical oceans in CMIP5 multi-climate models compared to CMIP3. *Clim. Dyn., 41*, 2909–2920, doi: 10.1007/s00382-013-1839-0.

Hirota, H., Y. N. Takayabu, M. Watanabe, M. Kimoto, and M. Chikira, 2014: Role of Convective Entrainment in Spatial Distributions of and Temporal Variations in Precipitation over Tropical Oceans. *J. Clim., 27*, 8707–8723.

Hwang, Y.-T. and D. M. W. Frierson, 2013: Link between the double-Intertropical Convergence Zone problem and cloud bias over Southern Ocean. *Proc. Nat. Acad. Sci., 110*, 4935–4940, doi: 10.1073/pnas.1213302110.

IPCC, 2013: *Climate Change 2013: The Physical Science Basis. Contribution of Working Group I to the Fifth Assessment Report of the Intergovernmental Panel on Climate Change* [Stocker, T.F., D. Qin, G.-K. Plattner, M. Tignor, S.K. Allen, J. Boschung, A. Nauels, Y. Xia, V. Bex and P.M. Midgley (eds.)]. Cambridge University Press, Cambridge, United Kingdom and New York, NY, USA, 1535 pp, doi:10.1017/CBO9781107415324.

Kiladis, G. N., H. von Storch, and H. van Loon, 1989: Origin of the South Pacific Convergence Zone. *J. Clim., 2*, 1185–1195, doi:10.1175/1520-0442.

Langenbrunner, B., J. D. Neelin, B. R. Lintner, and B. T. Anderson, 2015: Patterns of precipitation change and climatological uncertainty among CMIP5 models, with a focus on the midlatitude Pacific storm track. *J. Clim., 28,* 7857–7872, doi:10.1175/JCLI-D-14-00800.1.

Li, J., X. Zhang, Y. Yu, and F. Dai, 2004: Primary reasoning behind the double ITCZ phenomenon in a coupled ocean-atmosphere general circulation model. *Adv. Atmos. Sci., 21*, 857–867.

Li G, Xie S-P (2012) Origins of tropical-wide SST biases in CMIP multi-model ensembles. *Geophys. Res. Lett. 39*, L22703, doi:10.1029/2012GL05377.

Li, G., and S.-P. Xie, 2014: Tropical biases in CMIP5 multi-model ensemble: The excessive equatorial Pacific cold tongue and double ITCZ problems. *J. Clim., 27,* 1765–1780, doi: 10.1175/JCLI-D-13-00337.1.

Li, G., Y. Du, H. Xu, and B. Ren, 2015: An intermodel approach to identify the source of excessive equatorial Pacific cold tongue in CMIP5 models and uncertainty in observational datasets. *J. Clim.*, *28*, 7630–7640.

Li, G., S.-P. Xie, Y. Du, and Y. Luo, 2016: Effects of excessive equatorial cold tongue bias on the projections of tropical Pacific climate change. Part I: The warming pattern in CMIP5 multi-model ensemble. *Clim. Dyn.,* (in review).

Lin, J.-L., 2007: The double-ITCZ problem in IPCC AR4 coupled GCMs: Ocean-atmosphere feedback analysis. *J. Clim., 20*, 4497–4525.

Lintner, B. R., and J. D. Neelin, 2008: Eastern margin variability of the South Pacific Convergence Zone margin. *Geophys. Res. Lett.*, *35* (16), L16701, doi:10.1029/2008GL034298.

Mantsis, D. F., B. R. Lintner, A. J. Broccoli, and M. Khodri, 2013: Mechanisms of mid-Holocene precipitation change in the South Pacific Convergence Zone. *J. Clim., 26*, 6937–6953, doi:10.1175/JCLI-D-12-00674.1.

Matthews, A. J., 2012: A multiscale framework for the origin and variability of the South Pacific convergence zone. *Q. J. R. Meteorol. Soc*., *138*, 1165–1178.

Mechoso, C. R., and co-authors, 1995: The seasonal cycle over the tropical Pacific in coupled ocean-atmosphere general circulation models. *Mon. Weather Rev., 123*, 2825–2838.

Niznik, M. J., and B. R. Lintner, 2013: Circulation, precipitation, and moisture relationships along the South Pacific Convergence Zone in reanalyses and CMIP5 models. *J. Clim., 26,* 10174–10192, doi:10.1175/JCLI-D-13-00263.1.

Niznik, M. J., B. R. Lintner, A. J. Matthews, and M. J. Widlansky, 2015: The role of tropical–extratropical interaction and synoptic variability in maintaining the South Pacific Convergence Zone in CMIP5 Models. *J. Clim*., *28,* 3353–3374, doi:10.1175/JCLI-D-14-00527.1.

North, G. R., T. L. Bell, R. F. Cahalan, and F. J. Moeng, 1982: Sampling errors in the estimation of empirical orthogonal functions. *Mon. Wea. Rev., 110*, 699–706.

Oueslati, B., and G. Bellon, 2013: Convective Entrainment and Large-Scale Organization of Tropical Precipitation: Sensitivity of the CNRM-CM5 Hierarchy of Models. *J. Clim., 26*, 2931–2946, doi:10.1175/JCLI-D-12-00314.1.

Oueslati, B., and G. Bellon, 2015: The double ITCZ bias in CMIP5 models: interaction between SST, large-scale circulation and precipitation. *Clim. Dyn., 44*, 585–607, doi: 10.1007/s00382-015-2468-6.

Power, S., 2011: Understanding the South Pacific Convergence Zone and its impacts: International Workshop on the South Pacific Convergence Zone, Apia, Samoa, 24-26 August, 2010. *Eos, 92*, 55–56.

Siongco, A. C., C. Hohenegger, and B. Stevens, 2014: The Atlantic ITCZ bias in CMIP5 models. *Clim. Dyn., 5*, 1169–1180, doi: 10.1007/s00382-014-2366-3.

Takahashi, K., and D. S. Battisti, 2007: Processes controlling the mean tropical Pacific precipitation patterns: II. The SPCZ and southeast Pacific dry zone. *J. Clim., 20*, 5696–5706.

Taylor, K. E., R. J. Stouffer, and G. A. Meehl, 2012: An overview of CMIP5 and the experiment design. *Bull. Amer. Meteor. Soc., 93*, 485–498.

Vincent, D. G., 1994: The South Pacific Convergence Zone (SPCZ): A review. *Mon. Wea. Rev*., *122*, 1949–1970.

Xie, P., and P. A. Arkin, 1997: Global precipitation: A 17-year monthly analysis based on gauge observations, satellite estimates, and numerical model outputs. *Bull. Amer. Meteor. Soc., 78*, 2539–2558.

Wang, C., L. Zhang, S.-K. Lee, L. Wu, and C. R. Mechoso, 2014: A global perspective on CMIP5 climate model biases. *Nature Clim. Change, 4*, 201–205, doi:10.1038/nclimate2118.

Widlansky, M. J., A. Timmermann, K. Stein, S. McGregor, N. Schneider, M. H. England, M. Lengaigne, and W. Cai, 2013: Changes in South Pacific rainfall bands in a warming climate. *Nature Climate Change, 3*, 417–423, doi:10.1038/NCLIMATE1726.

Yin, X., A. Gruber, and P. A. Arkin, 2004: Comparison of the GPCP and CMAP Merged Gauge–Satellite Monthly Precipitation Products for the Period 1979–2001. *J. Hydrometeor., 5*, 1207–1222.

Zheng, Y., J.-L. Lin, and T. Shinoda, 2012: The equatorial Pacific cold tongue simulated by IPCC AR4 coupled GCMs: Upper ocean heat budget and feedback analysis. *J. Geophys. Res., 117*, C05024, doi:10.1029/2011JC007746.

Table and Figure Captions

Table 1: *List of model centers/groups and associated model acronyms analyzed.*

Figure 1: a) Model ensemble mean (MEM) DJF precipitation climatology for the 36 member CMIP5 historic simulation ensemble analyzed in the present study. The solid gray contour denotes the 4 mm day^{-1} precipitation isoline, which delineates the region of strongest deep convection in the Tropics. b) Departure of the MEM from Global Precipitation Climatology Project [GPCP; *Adler et al.* 2003] rainfall. The solid and dashed gray contours denote the 4 mm day^{-1} isolines from the MEM and GPCP, respectively.

Figure 2: 1st PUP of DJF-mean precipitation climatologies for the historic CMIP5 simulations. a) The 1st PUP spatial pattern (EOF), in units of mm day^{-1}. The solid and dashed contours represent the mm day^{-1} isolines for models with positive and negative loadings of this spatial pattern, respectively. Stippled areas pass the bootstrap significance test at the 99% confidence level (see text). b) Model weights (PCs) for mode 1, in units of standard deviation. Error bars represent the range of PC values that can arise from internal variability using model pre-industrial control runs (see text). c) Regression of the model's SST (shading) and 850 mb winds (vectors) based on the weights shown in b) and scaled by 1 standard deviation. Vectors are plotted when the regression slope of at least one component passes a two-sided test for difference from zero at the 95% confidence level.

Figure 3: As in Figure 2, but for the 2nd PUP.

Figure 4: Scatterplot of historic ensemble 1st PUP model weights (x-axis) versus 2nd PUP model weights (y-axis). The gray line depicts a quadratic polynomial best-fit curve to the data.

Figure 5: Leading PUP for maximum covariance analysis (MCA) applied to the DJF-mean cross-covariance matrix of normalized (a) precipitation and (b) SST for the N = 36 historic CMIP5 simulations. The top panel depicts the precipitation field (in units of mm day^{-1}) while the bottom panel depicts the SST field (in units of °C). Model weights for precipitation and SST (in units of standard deviation) appear in (c) and (d), respectively.

Figure 6: As in Figure 1, but for the 30 member AMIP-style ensemble.

Figure 7: 1st PUP of DJF-mean precipitation climatologies for the AMIP simulations. a) The 1st PUP spatial pattern (EOF), in units of mm day^{-1}. The solid and dashed contours represent the 4 mm day^{-1} isolines for models with positive and negative loadings of this spatial pattern, respectively. Vectors correspond to the regression of 850 mb winds on the weights shown in b). b) Model weights (PCs) for mode 1, in units of standard deviation.

Figure 8: (a) 1st and (b) 2nd PUP spatial patterns of DJF interannual precipitation standard deviations for the historic CMIP5 simulations, in units of mm day^{-1}. (c) 1st and (d) 2nd PUP model weights, in units of standard deviation.

Table 1: List of model centers/groups and associated model acronyms analyzed.

Modeling center/group/country	**Historic Ensemble acronym**	**Pre-industrial control length (years)**	**AMIP-ensemble acronym**
Commonwealth Scientific and Industrial Research Organization (CSIRO) and Bureau of Meteorology (BOM), Australia	ACCESS1-0	500	ACCESS1-0
	ACCESS1-3	500	ACCESS1-3
Beijing Climate Center, China Meteorological Administration	bcc-csm1-1	400	bcc-csm1-1
	bcc-csm1-1-m	500	bcc-csm1-1-m
Beijing Normal University	BNU-ESM	560	BNU-ESM
Canadian Centre for Climate Modelling and Analysis	CanESM2	1000	CanAM4
National Center for Atmospheric Research	CCSM4	1050	CCSM4
	CESM1-BGC	500	
	CESM1-CAM5	300	CESM1-CAM5
Centro Euro-Mediterraneo per I Cambiamenti Climatici	CMCC-CESM	275	
	CMCC-CM	300	CMCC-CM
	CMCC-CMS	500	
	CMCC-CM5	850	
Centre National de Recherches Météorologiques			CNRM-CM5
CSIRO with Queensland Climate Change Centre of Excellence	CSIRO-Mk3-6-0	500	CSIRO-Mk3-6-0
EC-EARTH consortium	EC-EARTH	450	EC-EARTH
LASG, Institute of Atmospheric Physics, Chinese Academy of Sciences	FGOALS-g2	700	FGOALS-g2
			FGOALS-s2
NOAA Geophysical Fluid Dynamics Laboratory	GFDL-CM3	500	GFDL-CM3
	GFDL-ESM2G	500	
	GFDL-ESM2M	500	
			GFDL-HIRAM-C180
			GFDL-HIRAM-C360
NASA Goddard Institute for Space Studies	GISS-E2-H	240	
	GISS-E2-R	550	GISS-E2-R
Met Office Hadley Centre (additional HadGEM2-ES realizations contributed by Instituto Nacional de Pesquisas Espaciais)			HadGEM2-A
	HadGEM2-AO	700	
	HadGEM2-CC	240	
	HadGEM2-ES	575	
Institute for Numerical Mathematics	inmcm4	500	inmcm4
Institut Pierre-Simon Laplace	IPSL-CM5A-LR	1000	IPSL-CM5A-LR
	IPSL-CM5A-MR	300	IPSL-CM5A-MR
	IPSL-CM5B-LR	700	IPSL-CM5B-LR
Japan Agency for Marine-Earth Science and Technology, Atmosphere and Ocean Research Institute (The University of Tokyo), and National Institute for Environmental Studies	MIROC5	700	MIROC5
	MIROC-ESM	530	

	MIROC-ESM-CHEM	250	
Max Planck Institute for Meteorology	MPI-ESM-LR	1000	MPI-ESM-LR
	MPI-ESM-MR	1000	MPI-ESM-MR
Meteorological Research Institute			MRI-AGCM3-2H
			MRI-AGCM3-2S
	MRI-CGCM3	500	MRI-CGCM3
Norwegian Climate Centre	NorESM1-M	250	NorESM1-M
	NorESM1-ME	500	

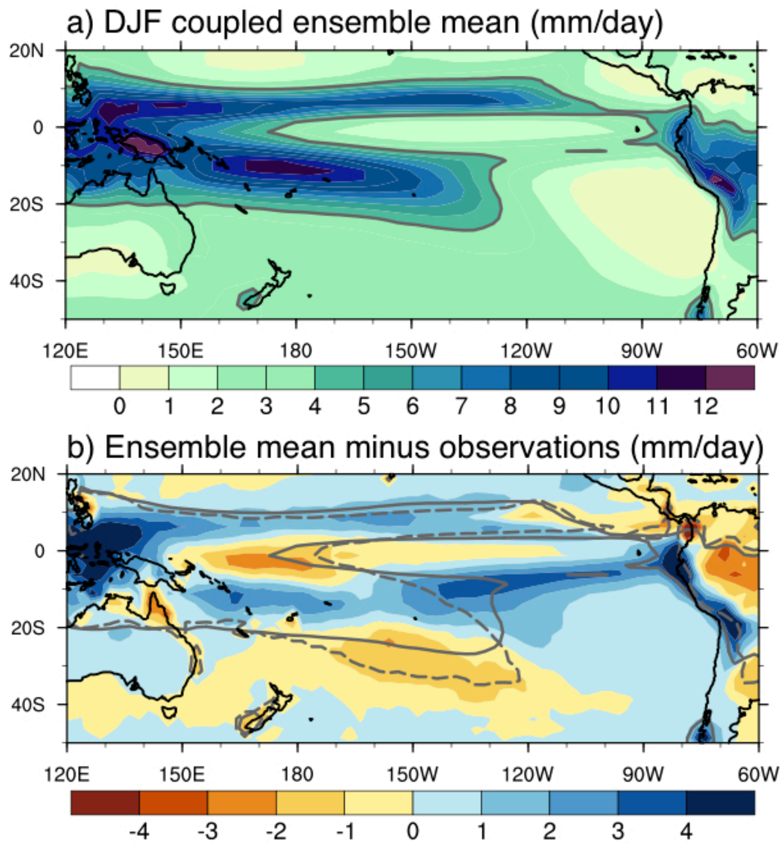

Figure 1: a) Model ensemble mean (MEM) DJF precipitation climatology for the 36 member CMIP5 historic simulation ensemble analyzed in the present study. The solid gray contour denotes the 4 mm day^{-1} precipitation isoline, which delineates the region of strongest deep convection in the Tropics. b) Departure of the MEM from Global Precipitation Climatology Project [GPCP; *Adler et al.* 2003] rainfall. The solid and dashed gray contours denote the 4 mm day^{-1} isolines from the MEM and GPCP, respectively.

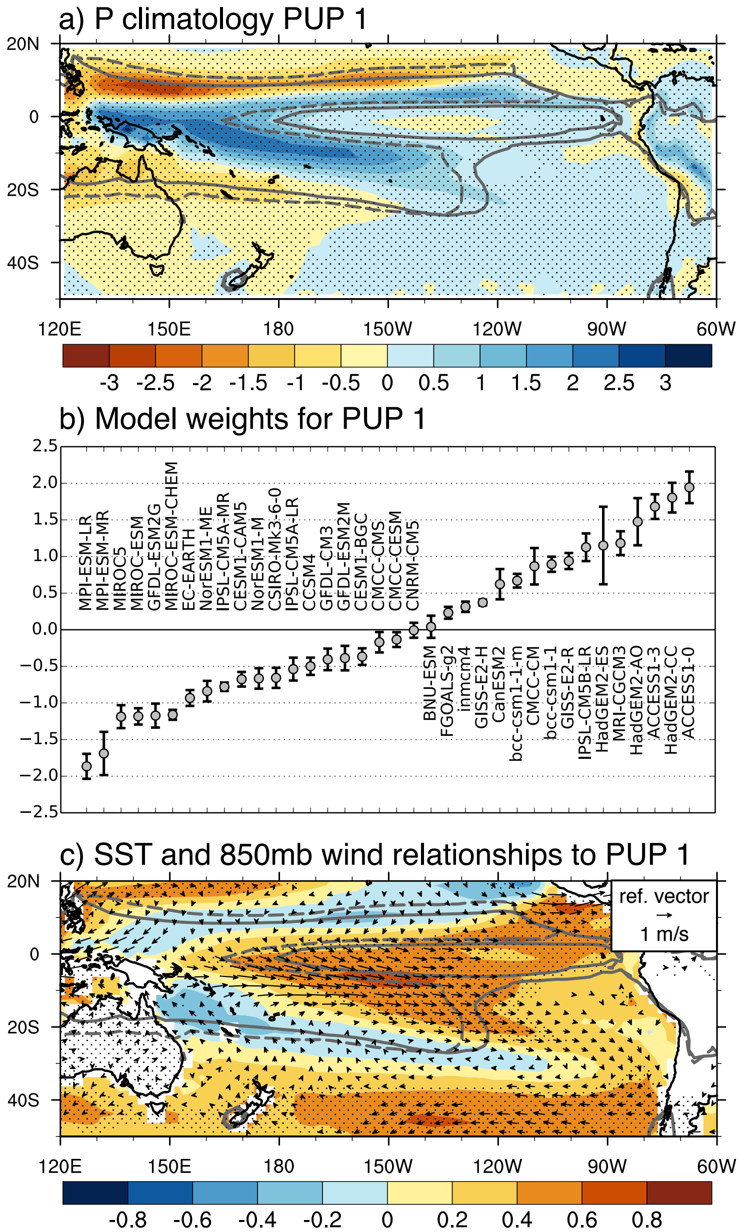

Figure 2: 1st PUP of DJF-mean precipitation climatologies for the historic CMIP5 simulations. a) The 1st PUP spatial pattern (EOF), in units of mm day^{-1}. The solid and dashed contours represent the mm day^{-1} isolines for models with positive and negative weights, respectively. Stippled areas pass the bootstrap significance test at the 99% confidence level (see text). b) Model weights (PCs) for PUP 1, in units of standard deviation. Error bars represent the range of weights that can arise from internal variability using model pre-industrial control runs (see text). c) Regression of the model's SST (shading) and 850 mb winds (vectors) based on the weights shown in b) and scaled by 1 standard deviation. Vectors are plotted when the regression slope of at least one component passes a two-sided test for difference from zero at the 95% confidence level.

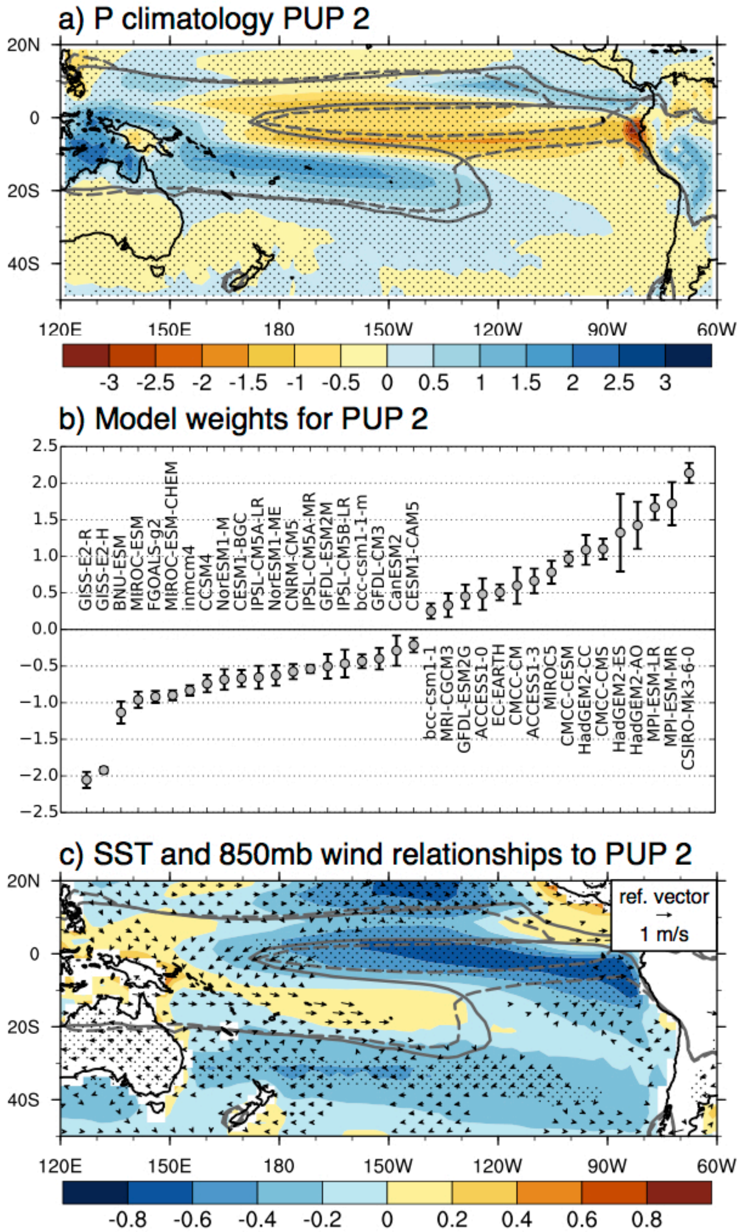

Figure 3: As in Figure 2, but for the 2nd PUP.

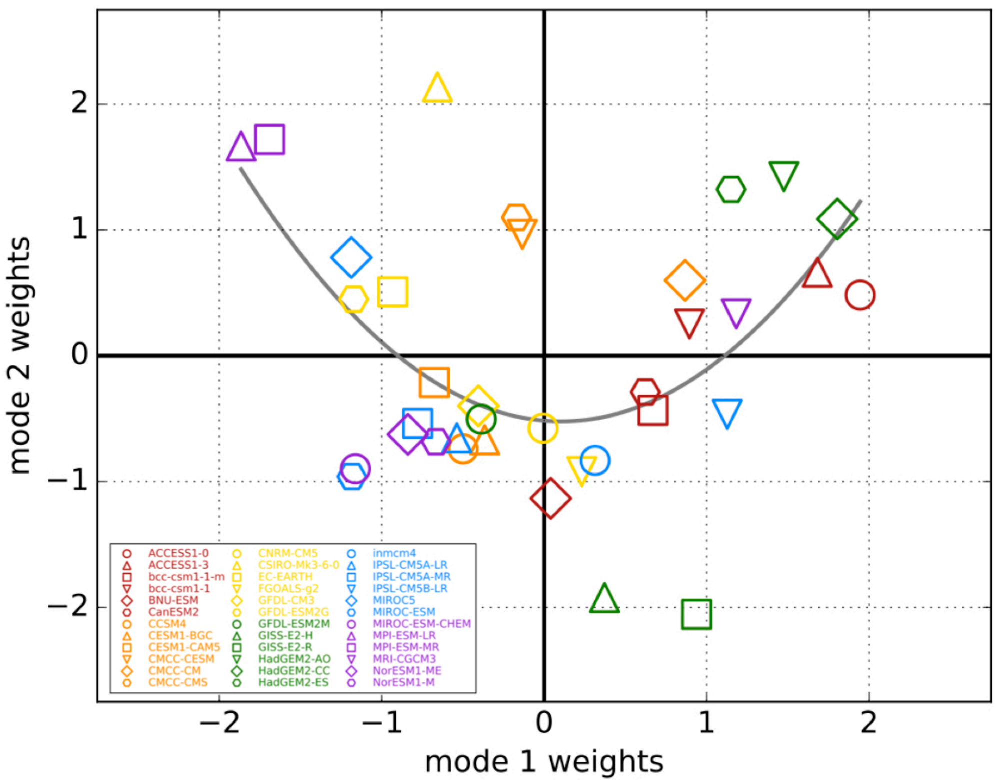

Figure 4: Scatterplot of historic ensemble 1st PUP model weights (x-axis) versus 2nd PUP model weights (y-axis). The gray line depicts a quadratic polynomial best fit curve to the data.

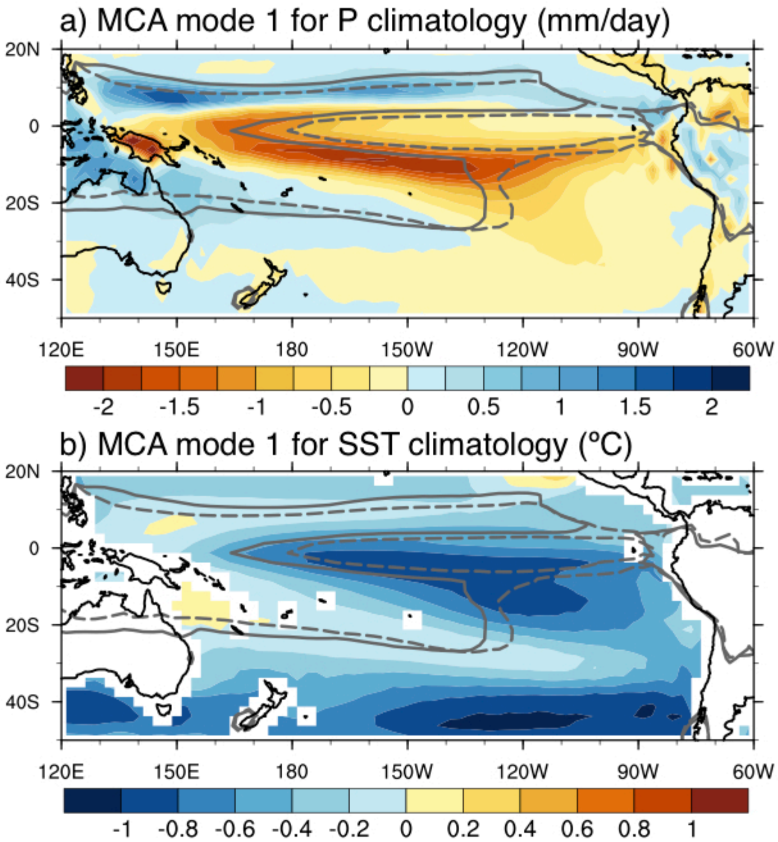

Figure 5: Leading PUP for maximum covariance analysis (MCA) applied to the DJF-mean cross-covariance matrix of normalized (a) precipitation and (b) SST for the N = 36 historic CMIP5 simulations. The top panel depicts the precipitation field (in units of mm day^{-1}) while the bottom panel depicts the SST field (in units of °C). Model weights for precipitation and SST (in units of standard deviation) appear in (c) and (d), respectively.

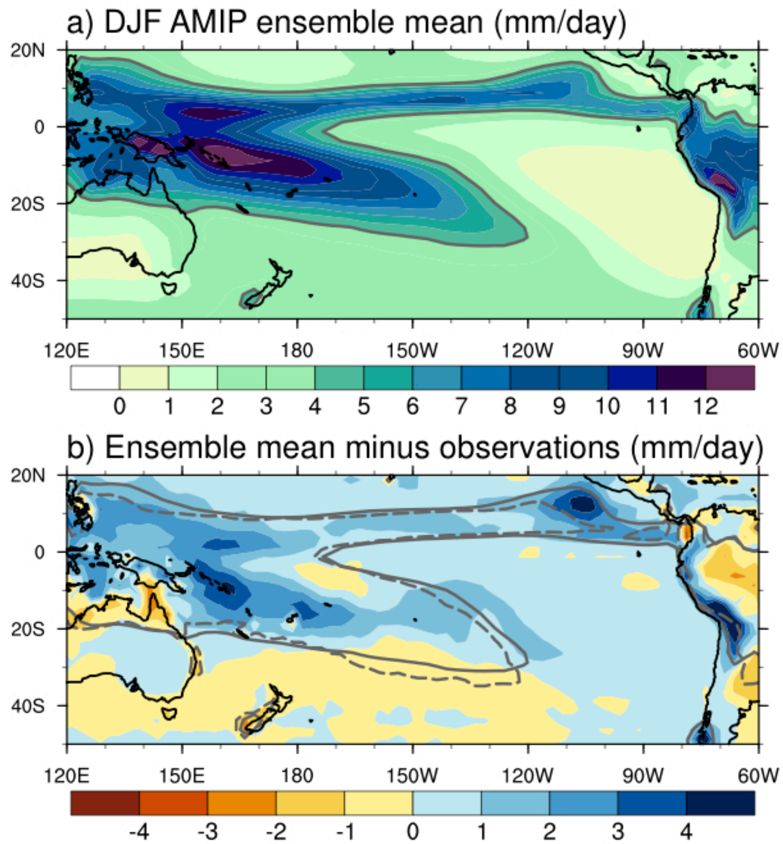

Figure 6: As in Figure 1, but for the 30 member AMIP-style ensemble.

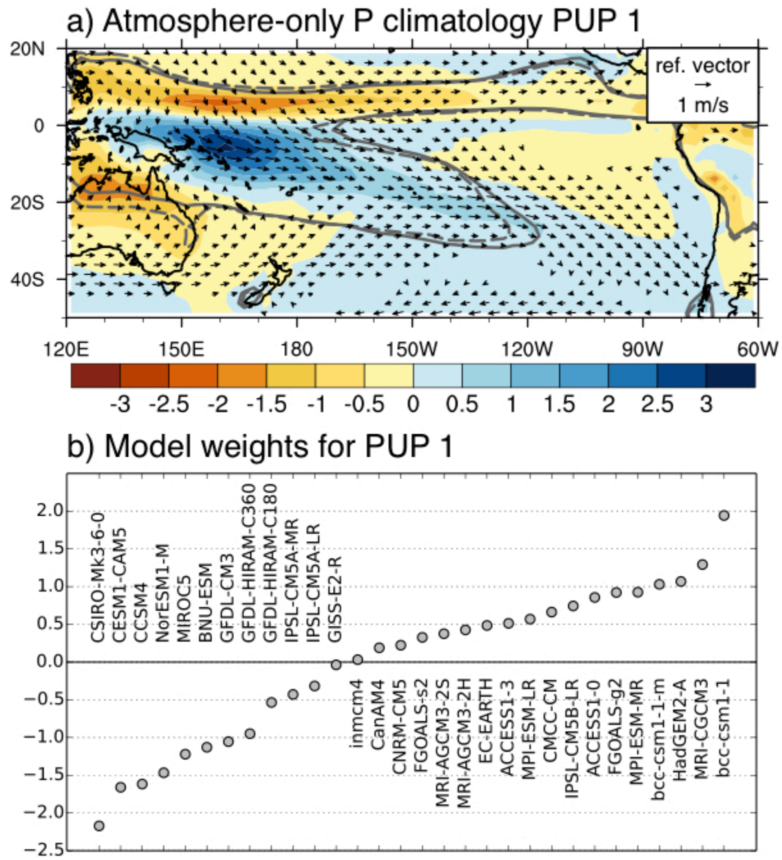

Figure 7: 1st PUP of DJF-mean precipitation climatologies for the AMIP simulations. a) The 1st PUP spatial pattern (EOF), in units of mm day^{-1}. The solid and dashed contours represent the 4 mm day^{-1} isolines for models with positive and negative loadings of this spatial pattern, respectively. Vectors correspond to the regression of 850 mb winds on the weights shown in b). b) Model weights (PCs) for mode 1, in units of standard deviation.

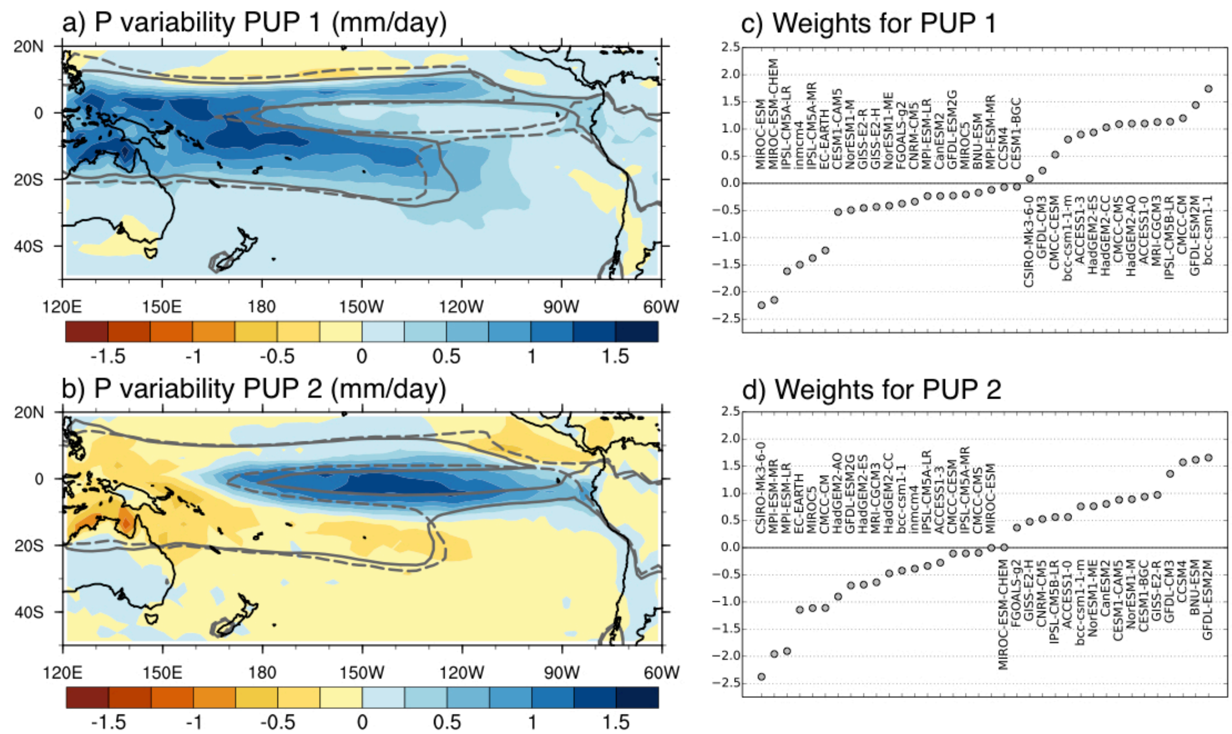

Figure 8: (a) 1st and (b) 2nd PUP spatial patterns of DJF interannual precipitation standard deviations for the historic CMIP5 simulations, in units of mm day^{-1}. (c) 1st and (d) 2nd PUP model weights, in units of standard deviation.